

# A new analysis of the MiniBooNE low-energy excess

C. Giunti,<sup>1,\*</sup> A. Ioannianian,<sup>2,3,4,†</sup> and G. Ranucci<sup>5,‡</sup>

<sup>1</sup>*Istituto Nazionale di Fisica Nucleare (INFN), Sezione di Torino, Via P. Giuria 1, I-10125 Torino, Italy*

<sup>2</sup>*CERN, Theory Division, CH-1211 Geneva 23, Switzerland*

<sup>3</sup>*Yerevan Physics Institute, Alikhanian Brothers 2, Yerevan-36, Armenia*

<sup>4</sup>*Institute for Theoretical Physics and Modeling, Yerevan-36, Armenia*

<sup>5</sup>*Istituto Nazionale di Fisica Nucleare (INFN), Sezione di Milano, I-20133 Milano, Italy*

(Dated: 3 December 2019)

We present the results of a new analysis of the data of the MiniBooNE experiment taking into account the additional background of photons from  $\Delta^{+0}$  decay proposed in Ref. [1]. We show that the new background can explain part of the MiniBooNE low-energy excess and the statistical significance of the MiniBooNE indication in favor of short-baseline neutrino oscillation decreases from  $5.1\sigma$  to  $3.3\sigma$ . We also consider the implications for short-baseline neutrino oscillations in the 3+1 active-sterile neutrino mixing framework. We show that the new analysis of the MiniBooNE data indicates smaller active-sterile neutrino mixing and may lead us towards a solution of the appearance-disappearance tension in the global fit of short-baseline neutrino oscillation data.

The MiniBooNE experiment [2] found a significant excess of low-energy  $\nu_e$ -like events that could be due to short-baseline  $\nu_\mu \rightarrow \nu_e$  oscillations generated by active-sterile neutrino mixing [3–5] or to other physics beyond the Standard Model [6–9]. The size of the low-energy MiniBooNE excess depends crucially on the estimated background. Among the different sources of background are the  $\Delta \rightarrow N\gamma$  photons produced by the decay  $\Delta^{+0} \rightarrow p/n + \gamma$  of  $\Delta^{+0}$ 's produced in neutral-current  $\nu_\mu$  interactions with the mineral oil ( $\text{CH}_2$ ) of the detector. Since in the MiniBooNE detector a single photon cannot be distinguished from an electron, the photons from  $\Delta^{+0}$  decay represent an intrinsic background in the search of  $\nu_e$  appearance from the  $\nu_\mu$  beam. The MiniBooNE collaboration estimated this background through the measurement of  $\pi^0$ 's that are produced by the decay  $\Delta^{+0} \rightarrow p/n + \pi^0$ , using the branching fractions [10, 11]

$$\text{Br}(\Delta^{+0} \rightarrow p/n + \gamma) = (6.0 \pm 0.5) \times 10^{-3}, \quad (1)$$

$$\text{Br}(\Delta^{+0} \rightarrow p/n + \pi^0) \simeq 2/3. \quad (2)$$

Final state interactions (FSI) cause the absorption of a fraction of the  $\pi^0$ 's in the carbon nucleus that was estimated of about 20% by the MiniBooNE collaboration [12]. However, in Ref. [1] one of us noted that measurements of  $\pi^0$  photoproduction on nuclei [13, 14] indicate that the fraction of  $\pi^0$ 's that emerge from the nucleus and can be observed is given by

$$\frac{N_{\pi^0}^{\text{FSI}}}{N_{\pi^0}^0} = \frac{\sigma_{\text{FSI}}(\gamma + {}^A\mathcal{N} \rightarrow \pi^0 + X)}{\sigma_0(\gamma + {}^A\mathcal{N} \rightarrow \pi^0 + X)} \simeq \frac{A^{2/3}}{A} = A^{-1/3}, \quad (3)$$

where  $A$  is the mass number of the target nucleus  ${}^A\mathcal{N}$ ,  $\sigma_{\text{FSI}}$  denotes the measured cross section which includes final state interactions and  $\sigma_0$  denotes the theoretical cross

section without final state interactions. Therefore, the number of  $\Delta^{+0}$  produced in neutral-current  $\nu_\mu$  interactions with  ${}^{12}\text{C}$  and the number of  $\gamma$ 's generated by their decay is a factor  $12^{1/3} \simeq 2.3$  larger than that obtained from the measurement of  $\pi^0$ 's without taking into account FSI. This enhancement of the  $\Delta \rightarrow N\gamma$  background due to  $\pi^0$  FSI is much larger than the 20% considered by the MiniBooNE collaboration [12].

The increase of the estimated  $\Delta \rightarrow N\gamma$  background due to the reevaluation of  $\pi^0$  FSI in  ${}^{12}\text{C}$  can explain in part the low-energy MiniBooNE excess, because its largest contribution occur in the lowest energy bins, as one can see from Figures 1(a) and 1(b) that reproduce the MiniBooNE event histograms in neutrino and antineutrino mode in Refs. [2, 15]. Taking into account the two protons in  $\text{CH}_2$ , we obtain that the  $\Delta \rightarrow N\gamma$  must be increases by a factor of about 1.8.

The effect of the  $\Delta \rightarrow N\gamma$  background in MiniBooNE was studied theoretically in Ref. [16], where it was found that the  $\Delta \rightarrow N\gamma$  background is a factor of about 2 larger than that estimated by the MiniBooNE collaboration. This is in rough agreement with our enhancement by a factor of about 1.8. On the other hand, the later theoretical studies in Refs. [17, 18] found an agreement with the MiniBooNE estimate. Since our approach is phenomenological, based on the experimentally motivated ratio (3) and the branching fractions (1) and (2), it is independent of the theoretical calculations of the absolute rate of  $\Delta \rightarrow N\gamma$  decays in MiniBooNE.

Figure 1 shows a comparison of the standard MiniBooNE event histograms (Figures 1(a) and 1(b)) with those obtained with our reevaluation of the effects of  $\pi^0$  FSI (Figures 1(c) and 1(d)). One can see that in the reproductions 1(a) and 1(b) of the original MiniBooNE histograms the low-energy bins show a large excess with respect to the background prediction. The excess is significantly reduced with our reevaluation of  $\pi^0$  FSI in  ${}^{12}\text{C}$  that visibly increase the  $\Delta \rightarrow N\gamma$  background. Only the first energy bin remains with a large visible excess.

The improvement of the fit of the MiniBooNE data

\* carlo.giunti@to.infn.it

† ara.ioannianian@cern.ch

‡ gioacchino.ranucci@mi.infn.it

is quantified by  $\chi^2/NDF = 32.4/22$ , corresponding to a goodness-of-fit of 7% obtained with  $A^{1/3} \pi^0$  FSI, compared to  $\chi^2/NDF = 53.0/22$ , corresponding to a goodness-of-fit of 0.02%, obtained in the standard analysis of MiniBooNE data.

The reevaluation of the low-energy MiniBooNE excess has important implications for the interpretation of the MiniBooNE data in terms of short-baseline neutrino oscillations due to active-sterile neutrino mixing. In the following we consider the 3+1 scenario in which in addition to the three standard light massive neutrinos  $\nu_1, \nu_2, \nu_3$ , with respective masses  $m_1, m_2, m_3$ , there is a heavier neutrino  $\nu_4$  with mass  $m_4$ . The masses of the three standard light massive neutrinos have small separations, determined by the measurements of solar, atmospheric and long-baseline oscillations:  $\Delta m_{21}^2 \simeq 7.4 \times 10^{-5} \text{ eV}^2$  and  $|\Delta m_{31}^2| \simeq 2.5 \times 10^{-3} \text{ eV}^2$ , with  $\Delta m_{ij}^2 \equiv m_i^2 - m_j^2$ . A much larger squared mass difference  $\Delta m_{41}^2 \simeq \Delta m_{42}^2 \simeq \Delta m_{43}^2 \gtrsim 0.1 \text{ eV}^2$  can generate short-baseline  $\bar{\nu}_\mu \rightarrow \bar{\nu}_e$  oscillations that may explain the LSND and MiniBooNE anomalies, as well as other indications of short-baseline neutrino oscillations [3–5]. The probability of short-baseline  $\bar{\nu}_\mu \rightarrow \bar{\nu}_e$  oscillations is given by

$$P_{\nu_\mu \rightarrow \nu_e}^{\text{SBL}(-)} = \sin^2 2\vartheta_{e\mu} \sin^2 \left( \frac{\Delta m_{41}^2 L}{4E} \right), \quad (4)$$

where  $E$  is the neutrino energy,  $L$  is the source-detector distance, and  $\sin^2 2\vartheta_{e\mu} = 4|U_{e4}|^2|U_{\mu 4}|^2$ , where  $U$  is the  $4 \times 4$  unitary mixing matrix.

Figure 2 shows a comparison of the standard allowed regions in the  $(\sin^2 2\vartheta_{e\mu}, \Delta m_{41}^2)$  plane obtained from the analysis of the MiniBooNE data and those obtained with our reevaluation of  $\pi^0$  FSI in  $^{12}\text{C}$ . The goodness-of-fit and the best-fit values of the oscillation parameters are listed in Table I, and the best fit event histograms are shown in Figure 1. The difference between the  $\chi_{\text{min}}^2$  with oscillations and the  $\chi^2$  without oscillations is 30.2 and 13.6, without and with  $A^{1/3} \pi^0$  FSI, respectively. Taking into account that there is a difference of two degrees of freedom corresponding to the two fitted oscillation parameters  $\sin^2 2\vartheta_{e\mu}$  and  $\Delta m_{41}^2$ , the statistical significance of the MiniBooNE indication in favor of oscillation decreases from  $5.1\sigma$  to  $3.3\sigma$  with the introduction of the  $A^{1/3} \pi^0$  FSI (the corresponding  $\chi^2$  probabilities of the background-only fit relative to the best oscillation fit are  $2.8 \times 10^{-7}$  and  $1.1 \times 10^{-3}$ )<sup>1</sup>.

From Figure 2 one can see that the allowed regions in the  $(\sin^2 2\vartheta_{e\mu}, \Delta m_{41}^2)$  plane change significantly by taking into account the effect of  $A^{1/3} \pi^0$  FSI. There is an extension of the allowed regions towards small values of the mixing parameter  $\sin^2 2\vartheta_{e\mu}$ . In particular, the best fit moves from a point with quasi-maximal mixing to a point with rather small mixing. This is beneficial, because large active-sterile mixing is disfavored by solar, atmospheric and long-baseline neutrino oscillation data [3–5].

The best-fit event histograms in Figure 1 show that the smaller number of signal events resulting from the smaller best-fit mixing that we obtained with  $A^{1/3} \pi^0$  FSI can fit well the data because of the increase of the background. Only the excess in the first bin is not well fitted. The values of the goodness-of-fit in Table I show that the fit of MiniBooNE data with  $A^{1/3} \pi^0$  FSI is better than the one without, although a close look at Figure 1 seems to indicate the opposite. The reason is that we fitted the data using the prescription of the MiniBooNE data release [19] where the covariance matrix takes into account the flux and cross section correlations between the uncertainties of the predicted  $\bar{\nu}_e$  events and the  $\bar{\nu}_\mu$  charged-current quasi-elastic events observed in MiniBooNE. Since the uncertainties of the  $\bar{\nu}_\mu \rightarrow \bar{\nu}_e$  signal are more correlated with the  $\bar{\nu}_\mu$  events than the background  $\bar{\nu}_e$ -like events and the  $\bar{\nu}_\mu$  events are very well fitted by the Monte Carlo prediction, it is better to fit the MiniBooNE data with the smaller  $\bar{\nu}_\mu \rightarrow \bar{\nu}_e$  signal and the larger background that we obtained with  $A^{1/3} \pi^0$  FSI.

It is interesting to compare the results of our new fit of the MiniBooNE data with the indication of the LSND experiment [20] in favor of short-baseline  $\bar{\nu}_\mu \rightarrow \bar{\nu}_e$  oscillations. Figure 3 shows a comparison of the combined LSND and MiniBooNE allowed regions in the  $(\sin^2 2\vartheta_{e\mu}, \Delta m_{41}^2)$  plane obtained without and with the effect of  $A^{1/3} \pi^0$  FSI. One can see that the changes are similar, but stronger, than those for MiniBooNE alone (shown in Figure 2): there is a clear shift of the allowed regions towards small mixing, with the absence of a  $1\sigma$  allowed region at large mixing. Although the best-fit point is at a large value of  $\Delta m_{41}^2$ , there is a  $1\sigma$  allowed region with the smallest mixing at  $\Delta m_{41}^2 \approx 2 \text{ eV}^2$ , that may be compatible with indications of short-baseline  $\bar{\nu}_e$  disappearance due to active-sterile neutrino mixing found in reactor experiments [4, 21–23].

Finally, we investigated the effects of the analysis of MiniBooNE data with  $A^{1/3} \pi^0$  FSI on the global fit of the data of short-baseline  $\bar{\nu}_\mu \rightarrow \bar{\nu}_e$  oscillation experiments. Besides MiniBooNE and LSND, we considered the data of the BNL-E776 [24], KARMEN [25], NOMAD [26], ICARUS [27] and OPERA [28] experiments, as done in Ref. [29]. Figure 4 shows a comparison of the global allowed regions in the  $(\sin^2 2\vartheta_{e\mu}, \Delta m_{41}^2)$  plane obtained without and with  $A^{1/3} \pi^0$  FSI in the analysis of MiniBooNE data. One can see that there is again a shift of the allowed regions towards small mixing. Although the

<sup>1</sup> In Ref. [2] the MiniBooNE collaboration obtained a probability of the background-only fit relative to the best oscillation fit of  $6 \times 10^{-7}$ , which corresponds to  $5.0\sigma$ . The small difference with our result is due to a different analysis of the data performed by the MiniBooNE collaboration with respect to that recommended in their data release [19]. In particular, they considered only the data below 1250 MeV because that upper limit “was chosen by the collaboration before unblinding the data in 2007” [2]. We have no reason to implement this restriction.

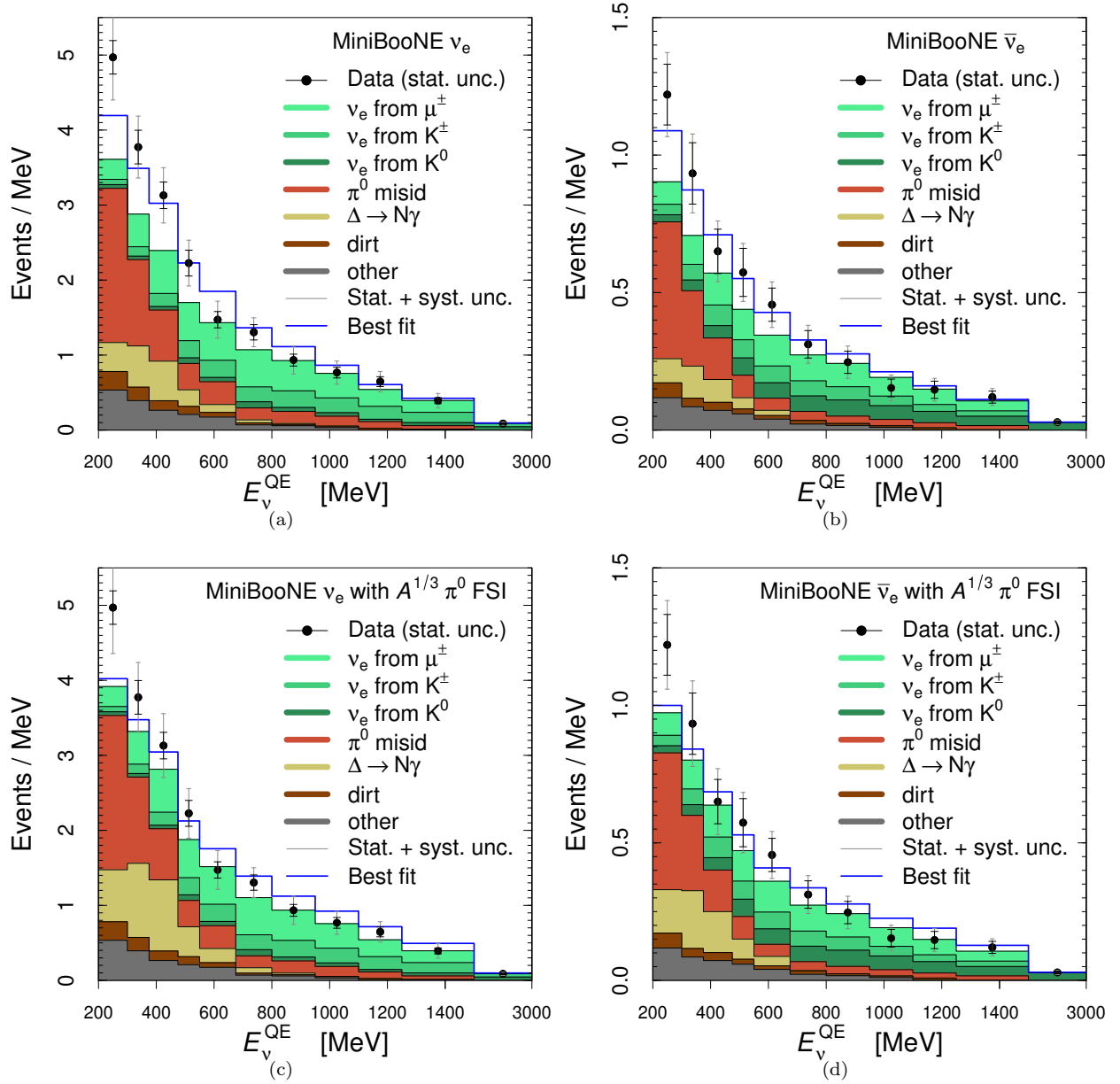


FIG. 1. Comparison of a reproduction of the MiniBooNE event histograms in (a) neutrino and (b) antineutrino mode from Refs. [2, 15] with our versions (c) and (d), which include the effect of  $A^{1/3} \pi^0$  FSI.

	MB	MB(FSI)	LSND+MB	LSND+MB(FSI)	App+MB	App+MB(FSI)
$\chi^2_{\min}$	22.8	18.9	29.5	28.2	81.1	76.7
NDF	20	20	25	25	69	69
GoF	30%	53%	24%	30%	15%	24%
$\Delta m_{41}^{2(\text{bf})}$	0.042	9.12	0.046	9.12	0.58	0.68
$\sin^2 2\theta_{e\mu}^{(\text{bf})}$	0.98	0.0023	1.00	0.0033	0.0065	0.0043

TABLE I. Minimum  $\chi^2$ , number of degrees of freedom (NDF) and Goodness of Fit (GoF) of the analyses of the data of short-baseline  $\nu_{\mu}^{(-)} \rightarrow \nu_e^{(-)}$  experiments discussed in the text without and with the effect of  $A^{1/3} \pi^0$  FSI in MiniBooNE (MB).  $\Delta m_{41}^{2(\text{bf})}$  and  $\sin^2 2\theta_{e\mu}^{(\text{bf})}$  are the best-fit values of the corresponding oscillation parameters.

shift of the best-fit point towards small mixings is not large, there is a much larger shift of the allowed regions,

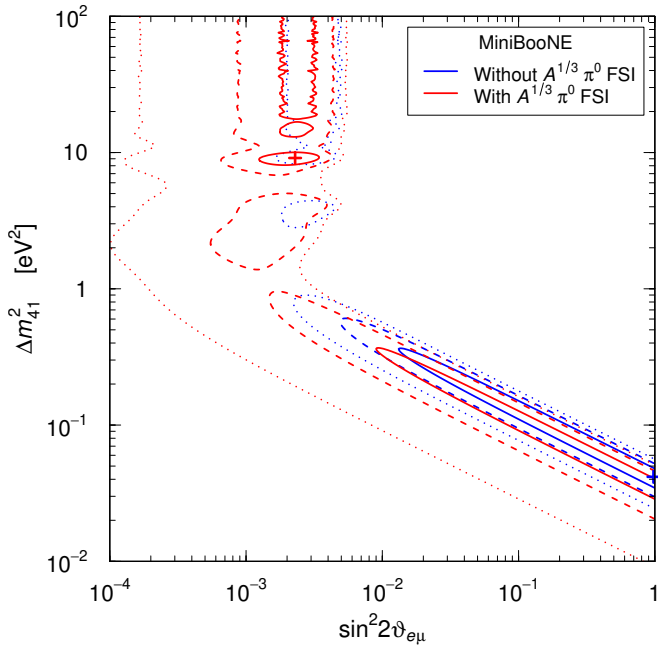


FIG. 2. Contours enclosing  $1\sigma$  (solid),  $2\sigma$  (dashed), and  $3\sigma$  (dotted) allowed regions in the  $(\sin^2 2\vartheta_{e\mu}, \Delta m_{41}^2)$  plane obtained from the analysis of MiniBooNE data without (blue) and with (red) the effect of  $A^{1/3} \pi^0$  FSI.

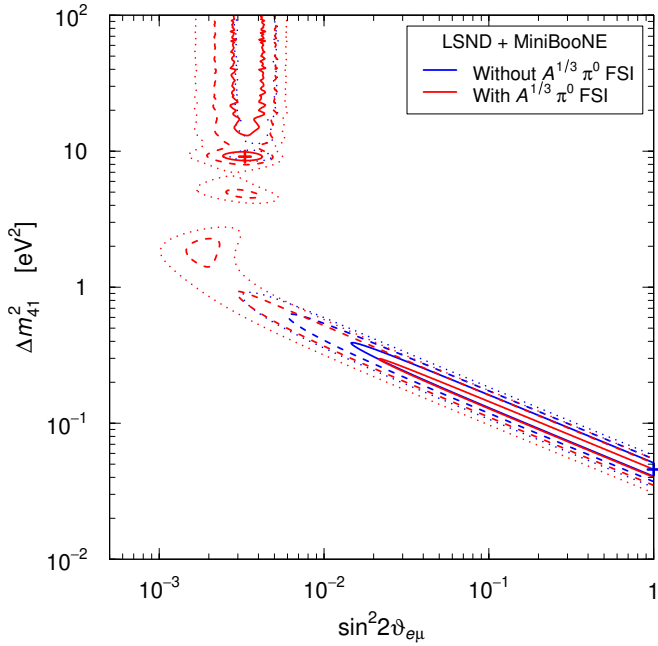


FIG. 3. Contours enclosing  $1\sigma$  (solid),  $2\sigma$  (dashed), and  $3\sigma$  (dotted) allowed regions in the  $(\sin^2 2\vartheta_{e\mu}, \Delta m_{41}^2)$  plane obtained from the analysis of LSND and MiniBooNE data without (blue) and with (red) the effect of  $A^{1/3} \pi^0$  FSI.

that reach  $\sin^2 2\vartheta_{e\mu} \approx 7 \times 10^{-4}$  at  $3\sigma$  for  $\Delta m_{41}^2 \approx 1.7 \text{ eV}^2$ . This shift is beneficial for a decrease of the appearance-disappearance tension in the global fit of short-baseline neutrino oscillation data in terms of 3+1 active-sterile

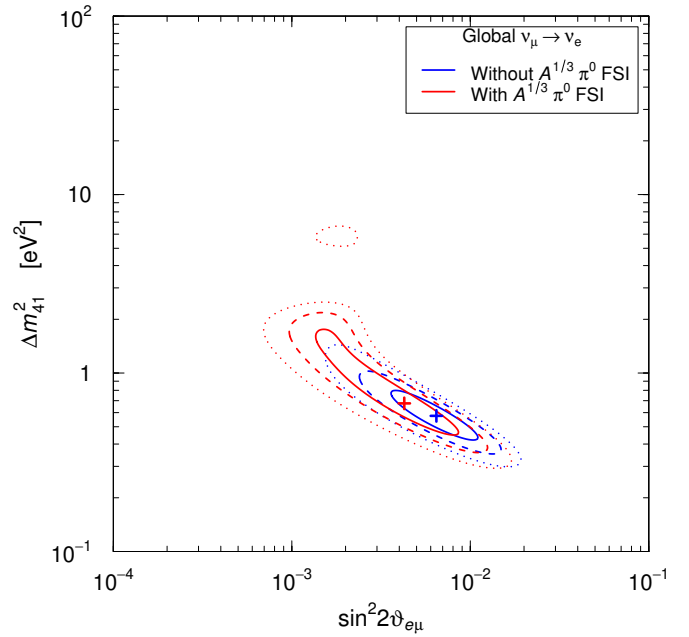


FIG. 4. Contours enclosing  $1\sigma$  (solid),  $2\sigma$  (dashed), and  $3\sigma$  (dotted) allowed regions in the  $(\sin^2 2\vartheta_{e\mu}, \Delta m_{41}^2)$  plane obtained from the global analysis of the data of  $(\bar{\nu}_{\mu} \rightarrow \bar{\nu}_e)$  oscillation experiments without (blue) and with (red) the effect of  $A^{1/3} \pi^0$  FSI in the analysis of MiniBooNE data.

neutrino mixing [21, 22, 29–42].

For example, the  $3\sigma$  upper limit from disappearance data in Figure 7 of Ref. [22] is about  $\sin^2 2\vartheta_{e\mu} \lesssim 6 \times 10^{-4}$  at  $3\sigma$  for  $\Delta m_{41}^2 \approx 1.3 \text{ eV}^2$ , that we can compare with the  $3\sigma$  lower limit  $\sin^2 2\vartheta_{e\mu} \gtrsim 8 \times 10^{-4}$  in Figure 4 for the same value of  $\Delta m_{41}^2$ . It is clear that there is still a considerable appearance-disappearance tension, but it is significantly smaller than that obtained in Ref. [22].

The disappearance bound in Figure 5b of Ref. [3] is weaker than that obtained in Ref. [22], with an upper limit  $\sin^2 2\vartheta_{e\mu} \lesssim 10^{-3}$  at  $3\sigma$  for  $\Delta m_{41}^2 \approx 1.3 \text{ eV}^2$ , that is compatible with the  $3\sigma$  allowed region in Figure 4.

In conclusion, we have shown that a reassessment of the photon background from  $\Delta^{+/\ 0}$  decay in the MiniBooNE experiment taking into account the effect of  $A^{1/3} \pi^0$  FSI proposed in Ref. [1] can explain in part the low-energy MiniBooNE excess and leads to a better fit of the data (with a goodness-of-fit of 7% compared to 0.02%, obtained in the standard analysis of MiniBooNE data) in absence of physics beyond the standard three-neutrino mixing. However, the MiniBooNE data are still fitted in a better way considering short-baseline  $(\bar{\nu}_{\mu} \rightarrow \bar{\nu}_e)$  oscillations due to active-sterile neutrino mixing, albeit the statistical significance of the indication in favor of oscillation decreases from  $5.1\sigma$  to  $3.3\sigma$ . We have shown that in the 3+1 framework the new analysis of the MiniBooNE data prefers small values of active-sterile neutrino mixing, in contrast with the large values preferred by the standard analysis of MiniBooNE data. This shift towards small

active-sterile neutrino mixing is beneficial towards a possible solution of the appearance-disappearance tension in the global fit of short-baseline neutrino oscillation data.

## ACKNOWLEDGMENTS

We would like to thank W.C. Louis and C.A. Ternes for useful discussions.

- 
- [1] A. Ioannisian, arXiv:1909.08571 [hep-ph].
- [2] A. A. Aguilar-Arevalo *et al.* (MiniBooNE), Phys.Rev.Lett. **121**, 221801 (2018), arXiv:1805.12028 [hep-ex].
- [3] C. Giunti and T. Lasserre, arXiv:1901.08330 [hep-ph].
- [4] A. Diaz, C. Argüelles, G. Collin, J. Conrad, and M. Shaevitz, arXiv:1906.00045 [hep-ex].
- [5] S. Boser, C. Buck, C. Giunti, J. Lesgourgues, L. Ludhova, S. Mertens, A. Schukraft, and M. Wurm, arXiv:1906.01739 [hep-ex].
- [6] E. Bertuzzo, S. Jana, P. A. N. Machado, and R. Z. Funchal, Phys.Rev.Lett. **121**, 241801 (2018), arXiv:1807.09877 [hep-ph].
- [7] P. Ballett, S. Pascoli, and M. Ross-Lonergan, arXiv:1808.02915 [hep-ph].
- [8] C. A. Argüelles, M. Hostert, and Y.-D. Tsai, arXiv:1812.08768 [hep-ph].
- [9] P. Coloma, Eur.Phys.J. **C79**, 748 (2019), arXiv:1906.02106 [hep-ph].
- [10] C. M. Ignarra, (2014), FERMILAB-THESIS-2014-31.
- [11] M. Tanabashi *et al.* (Particle Data Group), Phys. Rev. **D98**, 030001 (2018).
- [12] R. Dharmapalan, (2012), FERMILAB-THESIS-2012-29.
- [13] B. Krusche *et al.*, Eur. Phys. J. **A22**, 277 (2004), nucl-ex/0406002 [nucl-ex].
- [14] B. Krusche, Prog. Part. Nucl. Phys. **55**, 46 (2005), nucl-ex/0411033 [nucl-ex].
- [15] A. Aguilar-Arevalo *et al.* (MiniBooNE), Phys. Rev. Lett. **110**, 161801 (2013), arXiv:1303.2588 [hep-ex].
- [16] R. J. Hill, Phys. Rev. **D84**, 017501 (2011), arXiv:1002.4215 [hep-ph].
- [17] X. Zhang and B. D. Serot, Phys. Lett. **B719**, 409 (2013), arXiv:1210.3610 [nucl-th].
- [18] E. Wang, L. Alvarez-Ruso, and J. Nieves, Phys.Lett. **B740**, 16 (2015), arXiv:1407.6060 [hep-ph].
- [19] MiniBooNE Data Release for arXiv:1805.12028, [https://www-boone.fnal.gov/for\\_physicists/data\\_release/nue2018/](https://www-boone.fnal.gov/for_physicists/data_release/nue2018/).
- [20] A. Aguilar *et al.* (LSND), Phys. Rev. **D64**, 112007 (2001), hep-ex/0104049.
- [21] S. Gariazzo, C. Giunti, M. Laveder, and Y. F. Li, Phys.Lett. **B782**, 13 (2018), arXiv:1801.06467 [hep-ph].
- [22] M. Dentler, A. Hernandez-Cabezudo, J. Kopp, P. A. N. Machado, M. Maltoni, I. Martinez-Soler, and T. Schwetz, JHEP **1808**, 010 (2018), arXiv:1803.10661 [hep-ph].
- [23] J. Berryman and P. Huber, arXiv:1909.09267 [hep-ph].
- [24] L. Borodovsky *et al.* (BNL-E776), Phys. Rev. Lett. **68**, 274 (1992).
- [25] B. Armbruster *et al.* (KARMEN), Phys. Rev. **D65**, 112001 (2002), hep-ex/0203021.
- [26] P. Astier *et al.* (NOMAD), Phys. Lett. **B570**, 19 (2003), hep-ex/0306037.
- [27] M. Antonello *et al.* (ICARUS), Eur.Phys.J. **C73**, 2599 (2013), arXiv:1307.4699 [hep-ex].
- [28] N. Agafonova *et al.* (OPERA), JHEP **1307**, 004 (2013), arXiv:1303.3953 [hep-ex].
- [29] S. Gariazzo, C. Giunti, M. Laveder, and Y. F. Li, JHEP **1706**, 135 (2017), arXiv:1703.00860 [hep-ph].
- [30] N. Okada and O. Yasuda, Int. J. Mod. Phys. **A12**, 3669 (1997), hep-ph/9606411.
- [31] S. M. Bilenky, C. Giunti, and W. Grimus, Eur. Phys. J. **C1**, 247 (1998), hep-ph/9607372.
- [32] J. Kopp, M. Maltoni, and T. Schwetz, Phys. Rev. Lett. **107**, 091801 (2011), arXiv:1103.4570 [hep-ph].
- [33] C. Giunti and M. Laveder, Phys. Rev. **D84**, 073008 (2011), arXiv:1107.1452 [hep-ph].
- [34] C. Giunti and M. Laveder, Phys. Rev. **D84**, 093006 (2011), arXiv:1109.4033 [hep-ph].
- [35] C. Giunti and M. Laveder, Phys. Lett. **B706**, 200 (2011), arXiv:1111.1069 [hep-ph].
- [36] J. Conrad, C. Ignarra, G. Karagiorgi, M. Shaevitz, and J. Spitz, Adv.High Energy Phys. **2013**, 163897 (2013), arXiv:1207.4765 [hep-ex].
- [37] M. Archidiacono, N. Fornengo, C. Giunti, and A. Melchiorri, Phys. Rev. **D86**, 065028 (2012), arXiv:1207.6515 [astro-ph.CO].
- [38] M. Archidiacono, N. Fornengo, C. Giunti, S. Hannestad, and A. Melchiorri, Phys. Rev. **D87**, 125034 (2013), arXiv:1302.6720 [astro-ph.CO].
- [39] J. Kopp, P. A. N. Machado, M. Maltoni, and T. Schwetz, JHEP **1305**, 050 (2013), arXiv:1303.3011 [hep-ph].
- [40] C. Giunti, M. Laveder, Y. F. Li, and H. Long, Phys. Rev. **D88**, 073008 (2013), arXiv:1308.5288 [hep-ph].
- [41] S. Gariazzo, C. Giunti, M. Laveder, Y. F. Li, and E. Zavanin, J. Phys. **G43**, 033001 (2016), arXiv:1507.08204 [hep-ph].
- [42] M. Dentler, A. Hernandez-Cabezudo, J. Kopp, M. Maltoni, and T. Schwetz, JHEP **1711**, 099 (2017), arXiv:1709.04294 [hep-ph].